Transition to Pulsing Flow in Trickle-Bed Reactors Studied Using MRI

A. J. Sederman and L. F. Gladden
Dept. of Chemical Engineering, University of Cambridge, Pembroke Street, Cambridge, CB2 3RA, U.K.

DOI 10.1002/aic.10317
Published online January 14, 2005 in Wiley InterScience (www.interscience.wiley.com).

Ultrafast magnetic resonance imaging (MRI) is used to provide two-dimensional (2-D) images of gas-liquid distribution within trickle-bed reactors with data acquisition times of 20 and 40 ms. Gas-water, cocurrent downflow through a fixed bed of cylindrical porous pellets of length and dia. 3 mm, packed within a 43 mm internal dia. column, was studied in both the trickle- and pulsing-flow regimes. Superficial gas velocities in the range 50–345 mm s^{-1} (0.06–0.42 kg m^{-2} s^{-1}), and superficial liquid velocities in the range 0.4–13.3 mm s^{-1} (0.4–13.3 kg m^{-2} s^{-1}) were used. MRI is used to investigate the stability of the gas-liquid distribution in the trickle- and pulsing-flow regimes. At the onset of the transition to pulsing flow, local pulsing, at the length-scale of the size of the packing elements is observed within the bed. Increasing liquid velocity causes an increase in the number of these local pulses until a velocity is reached at which the system transforms to the rapidly-changing gas-liquid distribution typical of pulsing flow. © 2005 American Institute of Chemical Engineers *AIChE J,* 51: 615–621, 2005
Keywords: MRI, trickle-bed reactor, pulsing regime, hydrodynamics, two-phase flow

Introduction

Trickle-bed reactors usually consist of a fixed bed of catalyst particles, contacted by a gas-liquid two-phase flow, with cocurrent downflow as the most common mode of operation. Such reactors are particularly important in the petroleum industry where they are used primarily for hydrocracking, hydrodesulfurisation, and hydrodenitrogenation; other commercial applications are found in the petrochemical industry, involving mainly hydrogenation and oxidation of organic compounds. In an attempt to obtain a predictive understanding of the hydrodynamics of trickle beds, various tomographic methods have been used to investigate two-phase flow under trickle flow conditions. These measurement techniques include conductance and capacitance methods,[1-3] optical methods,[4-6] X-ray tomography,[7-10] and magnetic resonance imaging (MRI).[11-12] Excellent reviews of tomographic methods in chemical engineering are also available to the interested reader.[3,13] The motivation for much research in the development and application of tomographic methods in chemical engineering is to achieve fast data acquisition times such that transient phenomena can be studied. MRI has traditionally been used to provide relatively high spatial resolution images (30 –200 μm) at low data acquisition rates (that is, several minutes[11]). More recently, so-called "ultrafast" MRI methods, in which image acquisition times are typically 20 – 100 ms, have been implemented to study unsteady-state two-phase flows. Examples of this are the "real-time" imaging of bubble-train flow in a ceramic monolith using a modification of the RARE radio-frequency (r.f.) pulse sequence,[14] and a preliminary study of the stability of the gas-liquid distribution following a perturbation to the liquid flow rate during trickle-flow operation.[15] The focus of this article is to investigate the extent to which ultrafast MRI can be used to explore the stability of the gas-liquid distribution during trickle and pulsing flow, and more importantly, to investigate the extent to which MRI can yield information on the hydrodynamics in the pulsing regime and the nature of the transition from trickle-to-pulsing flow.

Trickle- and pulse-flow regimes are the contacting patterns most commonly encountered in commercial scale trickle beds

Correspondence for this article should be addressed to L. F. Gladden at Gladden@cheng.cam.ac.uk.

and, therefore, understanding the nature and characteristics of both the hydrodynamics in these flow regimes and the transitions between flow regimes are subjects of long-standing interest.[3,16-23] The flow pattern will significantly influence the performance of a given reactor through characteristics, such as phase holdups, power consumption and mass transfer fluxes, so successful modeling of trickle-bed reactors requires precise tools for the identification of the flow pattern to be expected for a specified set of operation conditions. An accurate prediction of the trickle-to-pulse transition is also of key importance in this regard.[22] Larachi et al.[22] have reported a detailed survey of all trickle-to-pulse flow transition models and correlations published between 1964 and 1997. On the basis of the database compiled in this review a correlation was then derived, from a neural network model, for predicting the trickle-to-pulse flow transition. As described by Larachi et al., there exist two conceptually different approaches for describing the onset of the pulsing regime, these being the microscopic and macroscopic models. Microscopic models or single-pore models analyze pore-scale hydrodynamics, and postulate that the macroscopic onset to pulse flow is an outcome of a statistically large number of local pulsatile occurrences.[16-18,21] In contrast, the macroscopic models analyze the onset of pulsing at the reactor scale from a stability analysis of first-principle volume-average Navier-Stokes equations.[19]

To date, the most detailed tomographic study of two-phase flow in trickle-bed reactors operating in the pulse-flow regime employed capacitance tomography[3] in which the time-scale between images was 15 ms, and the 3-D shape and extent of the pulse was studied for two-phase flow in a column of inner dia. 120 mm with a total packing length of 2 m. The packing elements used were porous spheres of dia. 3, 5 and 10 mm. Liquid holdup data from which a temporal autocorrelation function was calculated were obtained for liquid velocities either close to the transition to pulse flow or in the pulse-flow regime itself. In a previous MRI study we demonstrated the ability of magnetic resonance techniques to yield in-plane spatial resolution of 313 μm $\times$ 313 μm for a 1 mm slice section within a fixed bed of 5 mm spherical nonporous particles packed within a column of internal dia. 40 mm, from which measurements of liquid holdup and liquid-solid contact were obtained directly.[11] These measurements were made for two-phase flow in the trickle-flow regime for gas and liquid superficial velocities in the range 66–356 mm s^{-1} and 0.5 – 5.8 mm s^{-1}, respectively, corresponding to superficial mass velocities of 0.08 – 0.43 kg m^{-2} s^{-1}, and 0.5 – 5.8 kg m^{-2} s^{-1}. In this work, we report the implementation of an ultrafast MRI experiment that acquires 2-D images in a plane perpendicular to the direction of superficial flow, and demonstrate:

(1) During trickle flow, the gas-liquid distribution was found to be stable even at the fastest data acquisition times (20 ms) employed. This observation confirms that in the trickle-flow regime, longer image acquisition times, which would provide higher spatial resolution data from which estimates of, for example, catalyst wetting are obtained, do not average out any macroscopic spatial redistribution of liquid within the bed.

(2) In the pulsing-flow regime the gas-liquid distribution was found to vary with time, as expected, although evidence of correlations in the gas-liquid distribution up to ~40 ms are observed. Furthermore, preferred paths through the bed, at the size-scale of individual packing elements, are observed. Measurements of the variation in liquid holdup within the bed, as reflected by the ^{1}H signal intensity associated with the liquid phase, show evidence of liquid pulses moving through the bed. Preliminary analysis suggests that the frequency of these pulses is consistent with data reported by earlier workers using capacitance tomography[3] and conductance and anemometry[23] techniques.

(3) MRI is shown to be a sensitive probe of the liquid distribution within the bed and, as such, can be used to investigate changes in the gas-liquid distribution during the transition from trickle-to-pulsing flow. In particular, at the onset of the transition, local regions of pulsing are observed while the majority of the bed is still under conditions of constant gas-liquid distribution characteristic of the trickle-flow regime.

Experimental Methods

The trickle-bed column was constructed using a 700 mm long PTFE tube of internal dia. 43 mm. The packing elements used were cylindrical porous alumina pellets of length and dia. 3 mm, and porosity ~0.4. The pellets were presoaked in water for 24 h prior to the experiment in order to fully wet the pellets. The column was loaded to a height of 100 mm, and then tapped repeatedly to consolidate the packing. This procedure was repeated, each time increasing the height of the packing by 100 mm until the column was full. The bed was then operated in the pulsing-flow regime to further consolidate the bed over a period of several hours before MRI measurements were acquired. The liquid and gas used were water and air, respectively. A positive displacement liquid pump was used, and the flow rate was measured and controlled by rotameters, needle valves, and a recycle line. The trickle bed was operated under cocurrent downflow conditions. The liquid was fed to the bed through a distributor plate at the top of the PTFE column, and the gas flow was taken from a 6 barg oil-less airline and passed through a variable pressure reducer to 2 barg after which it was fed through a rotameter and needle valve. The gas entered the top of the column around the outside of the distributor plate. At the base of the column, a single line returned the liquid-gas mixture to a reservoir where the gas was released to the atmosphere. Pressure drop measurements were taken over a length of the packing of 680 mm at time intervals of 1 s and were logged for a period of 5 min. The center of the imaging section was approximately 500 mm below the distributor plate. Two-phase flow characteristics were studied for superficial gas and liquid velocities in the range 50–345 mm s^{-1} (0.06–0.42 kg $m^{-2}s^{-1}$) and 0.4–13.3 mm s^{-1} (0.4–13.3 kg $m^{-2}s^{-1}$), respectively. The combinations of gas and liquid velocities employed corresponded to conditions within both the trickle- and pulse- flow regimes, and included the transition region between these two regimes. The flow loop used is shown in Figure 1.

MRI experiments were performed on a Bruker Spectrospin DMX 200, 4.7 T magnet with a birdcage coil of length and dia. 6.3 cm. ^{1}H images were acquired at a frequency of 199.7 MHz. Spatial resolution was achieved using shielded gradient coils providing a maximum gradient strength of 13.90 G cm^{-1}. 2-D images were acquired in the plane perpendicular to the direction of superficial flow using a FLASH r.f. pulse sequence[24] with ramped gradients, shown in Figure 2. A pulse angle of 5° was used. A gaussian shaped soft pulse was used as the

slice-selective excitation pulse. The gradient echo time was 0.97 ms. All images reported here had a field-of-view of 45 mm × 45 mm. Images were acquired at two spatial (and temporal) resolutions. Data array sizes of 64 × 32 were acquired with an acquisition time of 40 ms, with an image slice thickness of 1 mm. Images acquired at lower spatial resolution, but higher temporal resolution had data array sizes of 32 ×16, with an acquisition time of 20 ms for a 2 mm slice thickness. Clearly, to acquire images at the faster rate, spatial resolution within the image has been sacrificed for increased time resolution. Images are acquired in immediate succession and, therefore, frame rates of 50 frames per s (f.p.s.) are achieved for the faster acquisition times employed here. The maximum number of images acquired in a single series was 540 and 140 for 32 × 16 and 64 ×32 data array sizes, respectively, this number being limited by hardware considerations. Note that given the gradient echo time of 0.97 ms and the T_2^* of the intraparticle liquid being ~ 300 μs, the intraparticle liquid contributes negligible signal intensity to the image.

Images of liquid distribution in the low interaction regime were recorded using both gradient and spin echo pulse sequences to observe the effect of T_2^*-susceptibility contrast on the image of the liquid distribution. While there were small differences in the absolute signal intensity between the images acquired using the two sequences, the spatial distribution of signal associated with the liquid was the same to within the limits of the spatial resolution of the data. Therefore, we are confident that the FLASH sequence is giving a robust measure of the liquid distribution, but we do not attempt to quantify the liquid holdup (that is, absolute liquid content within the image slice) from these data.

The experimental results are reported in the following order. First, the concept of the standard deviation map is introduced which allows us to demonstrate that the macroscopic gas-liquid distribution is constant down to time-scales of 20 ms in the trickle-flow regime. The maps of standard deviation quantify the extent to which a given pixel in an image within a particular slice section through the bed has a constant gas or liquid content within it over a period of time in which a number of

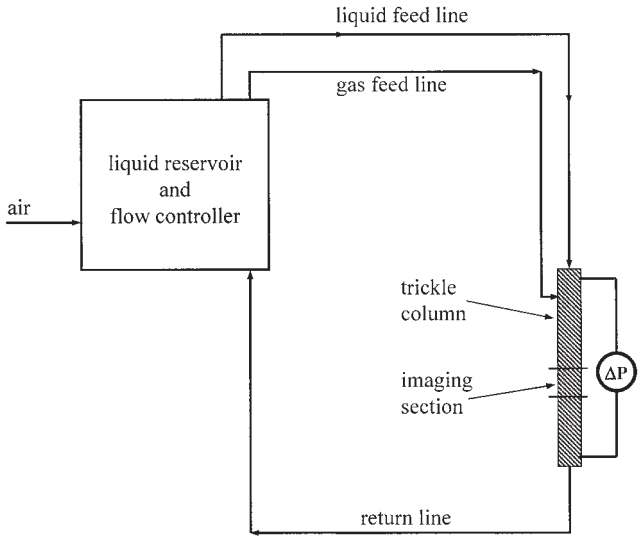

Figure 1. Flow loop.

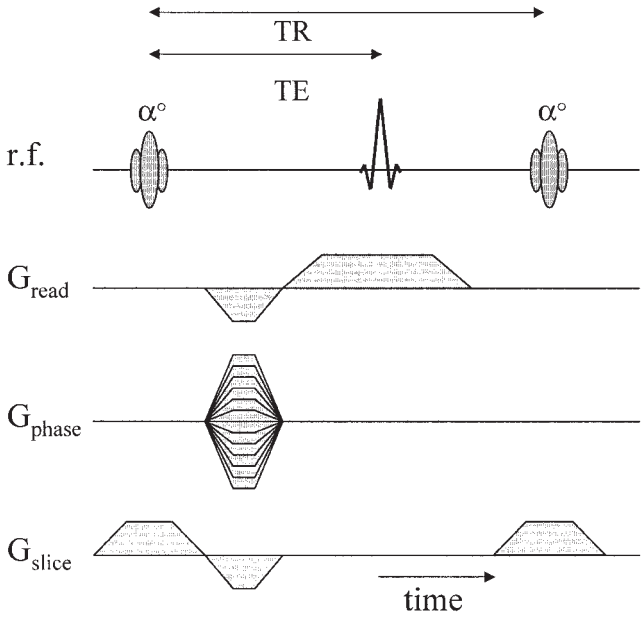

Figure 2. The FLASH r.f pulse sequence used in all MRI experiments.

TR and TE are the recycle time and echo time, respectively. α° represents the flip angle of the r.f. excitation pulse which is 5° in all experiments reported.

successive images are recorded. These maps of standard deviation are then compared for flows in the trickle and pulsing regimes. Second, hydrodynamics in the pulsing regime is considered in more detail. A series of images is shown which suggests that preferred paths for liquid slugs exist within the bed, and that a liquid "pulse" does not extend across the entire cross-section of the bed. Finally, the nature of the trickle-to-pulse transition is investigated using standard deviation maps. Measurements of effective liquid holdup as a function of time are also reported for increasing liquid velocities for two constant gas velocities.

The MRI data obtained have been analyzed using the following procedures; signal intensity in the images is acquired only from the liquid phase:

(1) *Standard deviation maps:* The simplest way to assess the stability of the gas-liquid distribution is to calculate a map of the standard deviation of the pixel intensities for each pixel in a time-series of images. Thus, for a series of n images, the standard deviation of the intensity associated with pixel i, σ_i, is calculated as follows

$$\sigma_i = \sqrt{\frac{\Sigma(x_i - \bar{x}_i)^2}{n}} \tag{1}$$

where x_i is the signal intensity of pixel i, $\bar{x}_i$ is the average intensity of pixel i in the series of n images; the summation being taken over the n images. Quantitative comparison of standard deviation maps obtained for different operating conditions is performed by calculating the average value of the standard deviation of the pixel intensities within each map.

(2) *Graphs of effective liquid holdup as a function of time:* This is calculated as the sum of liquid signal intensity in each

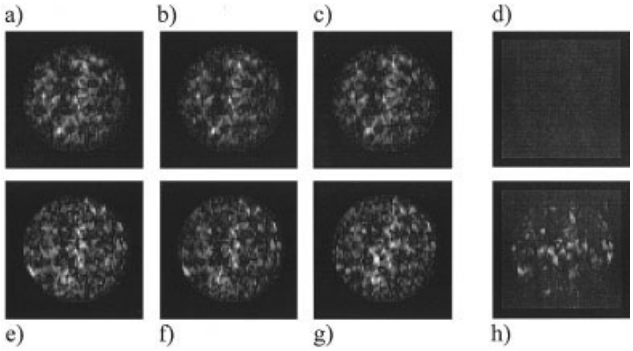

Figure 3. Evolution of gas-liquid distribution in the trickle- and pulsing-flow regimes.

(a-c) show images recorded in the trickle-flow regime, liquid and gas velocities are 1.2 and 50 mm s^{-1}, respectively; (e-g) show images recorded in the pulsing-flow regime, liquid and gas velocities are 9.7 and 50 mm s^{-1}, respectively. Each image took 40 ms to acquire and images were acquired in immediate succession. High intensity (white) corresponds to high liquid content. Signal intensity is associated only with the liquid phase. In-plane spatial resolution is 0.7 mm × 1.4 mm, and the image slice thickness is 1 mm. (d) and (h) are maps of the standard deviation calculated from 30 such images. Light and dark shades correspond to high and low values of standard deviation, respectively. The negligible intensity of the standard deviation map derived from images of the gas-liquid distribution in the trickle-flow regime indicates that on the time-scale of the measurements (that is, 40 ms), the gas-liquid distribution is stable within the image slice. Images (a)-(c), (e)-(g) are plotted on the same greyscale. Similarly, the two standard deviation maps ((d) and (h)) are plotted on the same greyscale, but different to that used for (a)-(c) and (e)-(g). The maximum value (white) of the greyscale used for the standard deviation maps is one third the value of the maximum value in the images of signal intensity.

of the images. As stated earlier, signal intensity is only acquired from liquid within the bed and, furthermore, the liquid holdups derived from the images are not quantitative because the FLASH r.f. pulse sequence will introduce contrast effects into the image which are difficult to quantify in such a complex system. In summary, the acquired images show us the liquid distribution and which volume elements in the bed contain liquid—but we make no attempt to quantify the amount of liquid within each image pixel, based on the signal intensity associated with that pixel. In addition to contrast effects inherent to use of this particular r.f. pulse sequence, the amount of signal from a volume element may also be affected by local contrast parameters. For example, a given image pixel might contain contributions to its signal intensity from both liquid in the inter-particle space, as well as a small contribution from liquid in the intraparticle space of the porous alumina pellets. Quantitative measurement of liquid holdup during trickle flow is possible by using "slow" spin-echo imaging techniques, which allow us to quantify relaxation time contrast effects in the data, and by accounting for local contrast variations arising from a given image voxel having contributions to its signal intensity from both intra- and interparticle space. The porous alumina pellets remain fully water-saturated throughout the experiment.

Results and Discussion

Figure 3 shows time-series of 3 successive images acquired in the trickle-flow (a-c), and pulse-flow (e-g) regimes. At the end of each series of images, the standard deviation map calculated from 30 such images is shown. It is clearly seen that the standard deviation map calculated from images acquired in the trickle-flow regime (d) has negligible intensity; that is, it is described by values of standard characteristic of the noise level in the images, suggesting that within the image series the gas-liquid distribution has remained constant to within the spatial resolution of the images. A similar standard deviation map is calculated from images acquired on the same bed saturated with water under conditions of zero flow. In contrast, the standard deviation map calculated from images acquired at the higher liquid flow velocity has significant pixel intensity throughout showing that the gas-liquid distribution varies over the time-scale of successive imaging experiments. Figure 4 shows a time-series of images recorded for gas-liquid flow rates characteristic of the pulse-flow regime. The gas and liquid superficial velocities are 50 mm s^{-1} and 9.7 mm s^{-1}, respectively. A series of 4 successive images is shown, each image has an acquisition time of 40 ms, recorded at regular intervals of 100 ms. The gas-liquid distribution differs markedly between these images. The highlighted region identifies a region of the bed in which a liquid pulse moves over the time-scale of the sequence of images. Although there is clearly a localized pulse in the highlighted region, this pulse does not extend across the cross section of the column, consistent with previously published capacitance tomography data[3] and studies of 2-D flat-bed reactors.[4,25] Images such as these can be used to identify preferred paths for liquid slugs within the fixed bed. Subsequent time frames to those shown here show liquid slugs moving repeatedly through the same highlighted region. The question then arises as to the time-scales over which there might exist any correlations in the gas-liquid distribution in the pulse-flow regime. The results of the analysis are shown in Figure 5. Each value plotted in Figure 5 is obtained by comparing the signal intensity, on a pixel-by-pixel basis, between two images, and then taking the standard deviation of this pixel value for all pairs of images separated by a specific time interval to form a standard deviation map from which an average is calculated. The point at t=40 ms, is calculated from the standard deviation map derived from images at, for example, t=0 and 40 ms, t=20, and 60 ms, and so on. In Figure 5, we see that, as expected, for two-phase flow in the trickle-flow regime, the average value of standard deviation characterising each map is constant and takes a low value, confirming a constant macroscopic gas-liquid distribution. Note that the

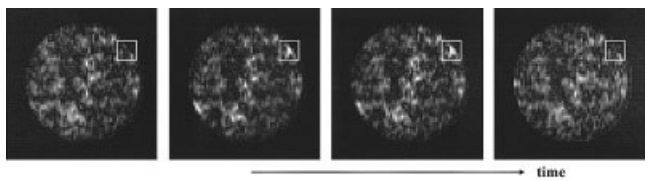

Figure 4. Movement of liquid slugs through local regions of the inter-particle space.

A series of 4 successive images is shown, each image has an acquisition time of 40 ms, recorded at regular intervals of 100 ms. The movement of liquid slugs through the highlighted region is clearly observed. Gas and liquid superficial velocities are 50 and 9.7 mm s^{-1}, respectively. In-plane spatial resolution is 0.7 mm × 1.4 mm, and the image slice thickness is 1 mm.

absolute value of standard deviation is arbitrary and will depend on the signal-to-noise of the image and the receiver gain settings. When the same data analysis procedure is applied to the images acquired in the pulse-flow regime, the standard deviation clearly increases as a function of time. This result suggests that over time-scales of 20–40 ms there are temporal correlations in the gas-liquid distribution; that is, a given pixel which is gas-filled at $t = t'$ has a significantly greater chance of being gas-filled at $t = t'+20$ ms. An interpretation of this observation is that a typical gas- or liquid-rich "slug" within the bed takes ~20–40 ms to move through the image slice. This is the subject of ongoing investigation. At time-scales of 60 ms and greater, the standard deviation begins to level off at a high value consistent with there being little correlation between whether a given pixel is gas or liquid filled over these longer time-scales.

Having considered conditions of gas and liquid flow velocity which lie in both the trickle and pulsing regime, we have used the same experimental and data analysis techniques to investigate the transition in hydrodynamics as the liquid velocity is increased, for a given gas velocity, from the trickle-to-pulsing regime. In Figure 6 we compare the evolution of (a) the MRI standard deviation maps through this transition with (b) the variation of pressure drop readings taken across the bed, and (c) the standard deviation of the pressure drop readings taken at 1 s intervals over a 5 min period for a given set of gas-liquid flow rates. The characteristics of the trickle-to-pulsing transition are considered in more detail in Figures 7 and 8. In Figure 7, the average standard deviation calculated as the average of the values in a given standard deviation map, such as those

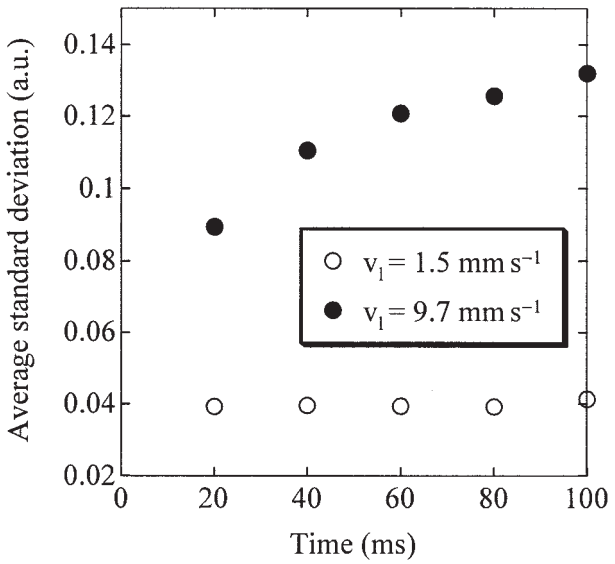

Figure 5. Identification of temporal correlations in the gas-liquid distribution.

The standard deviation between pairs of images acquired at increasing separation times is shown. In the trickle-flow regime, the low value of standard deviation between pairs of images confirms the stability of the distribution of gas and liquid within the bed. In the pulsing-flow regime, the standard deviation increases up to time-scales of ~100 ms, and is consistent with temporal correlations in the gas-liquid distribution existing over time-scales smaller than ~40 ms. Data are shown for a constant gas superficial velocity of 50 mm s^{-1}.

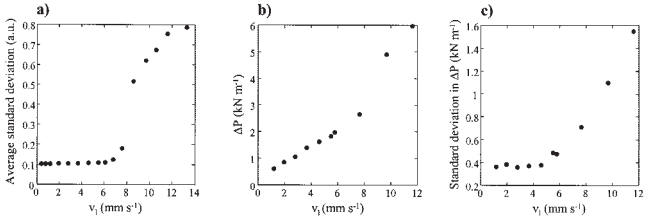

Figure 6. Comparison of MRI with pressure drop measurements during the trickling-to-pulsing flow transition.

Data are shown for a constant gas velocity of 50 mm s^{-1}. (a) The average standard deviation calculated from MRI standard deviation maps obtained at each liquid velocity; (b) pressure drop measurements made over the length of the whole bed; (c) the standard deviation in pressure drop measurements made over the length of the whole bed, and recorded at 1 s intervals over a 5 min period.

shown in Figure 3d and 3h is plotted as a function of liquid velocity for three different gas velocities. It is seen that as gas velocity is increased so the transition shifts to lower liquid velocity. The range of liquid velocities defining the transition region also appears to broaden with increasing gas velocity. The standard deviation maps also allow us to study changes in the gas-liquid distribution at the onset of the transition, as is shown in Figure 8. In Figure 8, standard deviation maps are shown for two constant gas velocities, 50 and 345 mm s^{-1}. For each gas velocity, standard deviation maps corresponding to four different liquid velocities are shown; liquid velocity increases left to right across the figure. At the lowest liquid velocities studied, the standard deviation map has intensities at the noise level, consistent with a constant gas-liquid distribution characteristic of the trickle-flow regime. At the highest liquid velocities studied in each case, the standard deviation map has a large number of high intensity (white) pixels, characteristic of fully pulsing flow. The second standard deviation map in each series (Figure 8b and 8f) corresponds to a liquid velocity of 4.6 mm s^{-1}, which lies at the lower bound of the transition from trickle-to-pulsing flow (see Figure 7). In these maps, isolated regions associated with a high value of standard deviation are observed, while the rest of the map remains at the noise level. These data strongly suggest that under these conditions, while most of the bed is still characterized by a constant macroscopic gas-liquid distribution (that is, associated with trickle flow), local pulsing is occurring within the bed. The length-scale over which local pulses occur is the typical size-scale of individual "pores" (that is, local regions of the interparticle space of size-scale typical of that of the packing elements) forming the bed. As liquid velocity is increased, so the number of local pulses increases. This is supported by comparing Figures 8b and 8f. For the higher gas velocity (Figure 8f), the liquid velocity of 4.6 mm s^{-1} lies further into the transition than is the case for the lower gas velocity (Figure 8b); that is, in Figure 8f, three extended local pulsing regions are seen compared to only 1 single-pixel "pulse" in Figure 8b. Combining these observations with the data shown in Figure 7 suggests that as liquid velocity is further increased, a liquid velocity is reached at which a sharp transition occurs from local pulsing to a rapidly changing gas-liquid distribution throughout the bed. Videos created from a time series of images recorded during trickle and pulsing flow, as well as at one set of

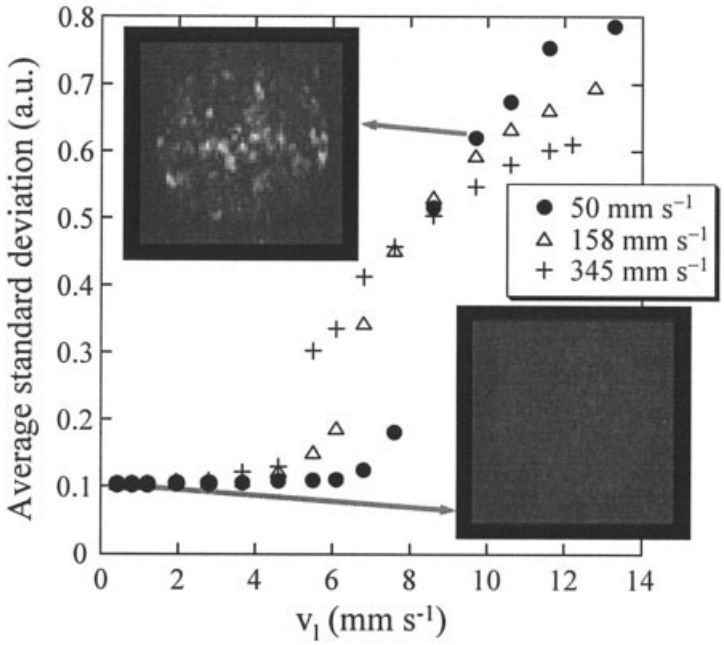

Figure 7. Effect of gas velocity on the trickle-to-pulse transition.

The average standard deviation calculated from MRI standard deviation maps obtained at each liquid velocity is shown for three different gas velocities. Typical standard deviation maps from which these values are calculated are also shown. As gas velocity decreases, so the onset of pulsing moves to higher liquid velocities and occurs over a narrower range of liquid velocities.

conditions at the transition can be found on the Web at http://www.cheng.cam.ac.uk/groups/mri/aichej.htm.

Comparison of the data shown in Figure 8a-8d and Figure 6 suggests that the standard deviation in the pressure drop measurements is particularly sensitive to the local pulsing which occurs at the onset of the hydrodynamic transition. The MRI analysis (Figure 6a) is less sensitive to the initial local pulsing, because the experiment is only sampling the hydrodynamics within a narrow slice section through the bed and, given the small size-scale of the local pulses, a single pulsing region will give only a marginal increase to the overall intensity of the MRI standard deviation map. However, the suddenness of the transition to fully pulsing flow (that is, rapidly changing gas-liquid distribution throughout the bed) is far more clearly seen in the MRI data than in the pressure drop measurements. A more detailed investigation of the evolution of the hydrodynamics during the trickle-to-pulsing transition is currently being performed, including the possible contribution of flow-induced contrast effects on the absolute magnitude of the values of the standard deviation obtained. However, these initial results support strongly the "microscopic" theoretical treatments of the flow regime transition in which local instabilities are first created from which the full transition to pulsing flow follows.

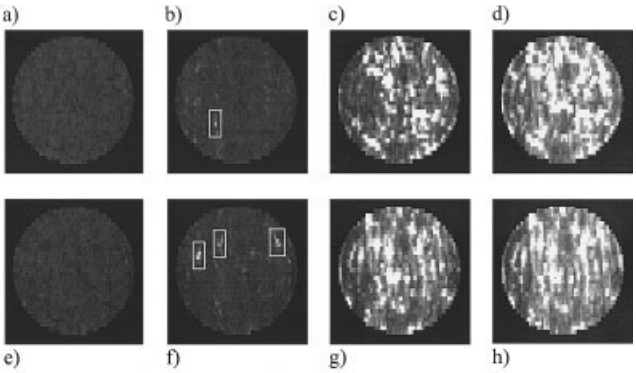

Figure 8. Identification of local pulsing at the onset of the transition from trickle to pulsing flow.

Standard deviation maps are shown for two gas velocities as a function of increasing liquid velocity. Standard deviation maps are calculated from a series of 128 individual images of the gas-liquid distribution under that specific set of flow conditions. Images were acquired with in-plane spatial resolution of 0.7 mm × 1.4 mm, and an image slice thickness of 1 mm; image acquisition time was 40 ms. (a-d) show standard deviation maps for a constant gas velocity of 50 mm s^{-1}; liquid velocities are (a) 1.2, (b) 4.6, (c) 9.7, and (d) 13.3 mm s^{-1}. (e-h) show data for a gas velocity of 345 mm s^{-1}; liquid velocities are (a) 1.2, (b) 4.6, (c) 9.7, and (d) 12.2 mm s^{-1}. Regions of local pulsing are highlighted in (b) and (f).

Figure 9 shows the effective liquid holdup for two constant gas velocities, 50 and 345 mm s^{-1}, each for 5 different liquid velocities. In both Figures 9a and 9b, for the liquid velocities at which the standard deviation maps shown in Figure 8, suggest a constant gas-liquid distribution, the effective liquid holdup, as measured by the signal intensity within the image, is constant. At the highest liquid velocities studied, for both gas flow velocities, variations in the liquid holdup with time are observed, consistent with the concept of liquid pulses moving through the bed. As soon as any local pulsing effects are observed in the standard deviation maps, so the signal intensity shows deviations from a constant signal intensity (that is, liquid holdup) as a function of time. Overall, as liquid velocity increases for a constant gas velocity the liquid holdup increases until the pulsing regime is established after which point the "base line" liquid holdup remains approximately constant and

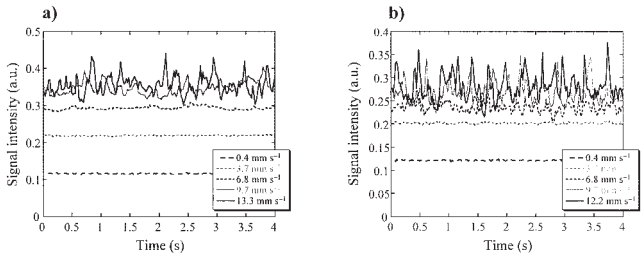

Figure 9. Effective liquid holdup, calculated by integrating the signal intensity across the entire image slice, for constant gas velocities of (a) 50 mm s^{-1}, and (b) 345 mm s^{-1}, for five different liquid velocities.

additional liquid is carried by the liquid pulses. Preliminary analysis of these data suggest that the frequency of these pulses is consistent with data reported previously for similar beds using capacitance tomography[3] and conductance and anemometry[23] techniques. Analysis of temporal autocorrelations characterising the pulsing phenomena observed in our data is the subject of ongoing investigation.

Conclusions

Ultrafast MRI techniques have been used to acquire 2-D images of gas-liquid distribution within fixed-bed reactors operating under a range of gas and liquid velocities in two-phase cocurrent downflow. These images confirm that down to the fastest data acquisition times considered (20 ms) the macroscopic gas-liquid distribution during trickle flow is constant. Standard deviation maps calculated from a time-series of 2-D images were then used to quantify the stability of the gas-liquid distribution as liquid velocity was increased at a constant gas velocity. In particular, we have shown that MRI has sufficient spatial resolution to study the transition in hydrodynamics as the system moves from the trickling to pulsing regime. It has been observed that as the system first deviates from the stable gas-liquid distribution characteristic of trickle flow, local liquid pulsing occurs over length-scales typical of the size of the packing elements. As liquid velocity increases, so the number of such local pulsing regions increases until the system rapidly transforms to hydrodynamics characteristic of the pulsing regime. This work represents a preliminary study illustrating the opportunities for applying MRI techniques in this application. A more detailed study of the changes in hydrodynamics during the trickle-to-pulse regime transition, under a range of experimental conditions, is ongoing.

Acknowledgments

We acknowledge the Innovative Manufacturing Initiative, Accelrys, Ltd., BP plc, Johnson Matthey plc, Grace Davison GMBH and Robinson Brothers, Ltd. for financial support of this work. We also thank Dr. P. Alexander for useful discussions.

Literature Cited

1. Helwick JA, Dillon PO, McCready MJ. Time-varying behaviour of cocurrent gas-liquid flows in packed-beds. *Chem. Eng. Sci*. 1992;47:3249-3256.
2. Krieg DA, Helwick JA, Dillon PO, McCready MJ. Origin of disturbances in cocurrent gas-liquid packed-bed flows. *AIChE J*. 1995;41:1653-1666.
3. Reinecke N, Mewes D. Investigation of the two phase flow in trickle-bed reactors using capacitance tomography. *Chem. Eng. Sci*. 1997;52:2111-2127.
4. Melli TR, de Santos JM, Kolb WB, Scriven LE. Cocurrent downflow in networks of passages - microscale roots of macroscale flow regimes. *Ind. Eng. Chem. Res*. 1990;29:2367-2379.
5. Kolb WB, Melli TR, de Santos JM, Scriven LE. Cocurrent downflow in packed beds. Flow regimes and their acoustic signals. *Ind. Eng. Chem. Res*. 1990;29:2380-2389.
6. Tsochatzidis NA, Karabelas AJ. Experiments in trickle beds at the microscale and macroscale - flow characterization and onset of pulsing. *Ind. Eng. Chem. Res*. 1994;33:1299-1309.
7. Nakamura M, Mori H, Hori F, Kitao T, Adachi Y, Toyama S. Vizualization of liquid flow in trickle bed reactor by X-ray computer tomography method. *Proc. of The Int. Conf. on Multiphase Flow*, Tsukuba, Japan. 1991.
8. Kantzas A. Computation of holdups in fluidized and trickle beds by computer-assisted tomography. *AIChE J*. 1994;40:1254-1261.
9. Toye D, Marchot P, Crine M, L'Homme G. Analysis of liquid flow distribution in trickling flow reactor using computer-assisted X-ray tomography. *Chem. Eng. Res. Des.* 1995;73:258-262.
10. Toye D, Marchot P, Crine M, L'Homme G. Modeling of multiphase flow in packed-beds by computer-assisted X-ray tomography. *Meas. Sci. Technol*. 1996;7:436-443.
11. Sederman AJ, Gladden LF. Magnetic resonance imaging as a quantitative probe of gas-liquid distribution and wetting efficiency in trickle-bed reactors. *Chem. Eng. Sci.* 2001;56:2615-2628.
12. Gladden LF, Lim MHM, Mantle MD, Sederman AJ, Stitt EH. MRI visualisation of two-phase flow in structured supports and trickle-bed reactors. *Catal. Today*. 2003;79:203-210.
13. Chaouki J, Larachi F, Dudukovic MP. Noninvasive tomographic and velocimetric monitoring of multiphase flows. *Ind. Eng. Chem. Res*. 1997;36:4476-4503.
14. Mantle MD, Sederman AJ, Gladden LF, Raymahasay S, Winterbottom JM, Stitt EH. Dynamic MRI visualization of two-phase flow in a ceramic monolith. *AIChE J*. 2002;48:909-912.
15. Gladden LF, Alexander P, Britton MM, Mantle MD, Sederman AJ, Yuen EHL. *In situ* magnetic resonance measurement of conversion, hydrodynamics and mass transfer during single- and two-phase flow in fixed-bed reactors. *Magn. Reson. Imaging*. 2003;21:213-219.
16. Sicardi S, Hofmann H. Influence of gas velocity and packing geometry on pulsing inception in trickle-bed reactors. *Chem. Eng. J*. 1980;20:251-253.
17. Blok JR, Varkevisser J, Drinkenburg AAH. Transition to pulsing flow, holdup and pressure drop in packed columns with cocurrent gas-liquid downflow. *Chem. Eng. Sci.* 1983;38:687-699.
18. Ng KM. A model for flow regime transitions in cocurrent down-flow trickle-bed reactors. *AIChE J*. 1986;32:115-122.
19. Grosser K, Carbonell RG, Sundaresan S. Onset of pulsing in two-phase cocurrent downflow through a packed bed. *AIChE J*. 1988;34:1850-1860.
20. Dankworth DC, Kevrekidis IG, Sundaresan S. Dynamics of pulsing flow in trickle beds. *AIChE J*. 1990;36:605-621.
21. Holub RA, Duduković MP, Ramachandran PA. A phenomenological model for pressure drop, liquid holdup, and flow regime transition in gas-liquid trickle flow. *Chem. Eng. Sci.* 1992;47:2343-2348.
22. Larachi F, Iliuta I, Chen M, Grandjean BPA. Onset of pulsing in trickle beds: evaluation of current tools and state-of the-art correlation. *Can. J. Chem. Eng*. 1999;77:751-758.
23. Boelhouwer JG, Piepers HW, Drinkenburg AAH. Nature and characteristics of pulsing flow in trickle-bed reactors. *Chem. Eng. Sci*. 2002;57:4865-4876.
24. Haase A, Frahm J, Matthaei D, Hanicke W, Merboldt KD. Flash imaging - rapid NMR imaging using low flip-angle pulses. *J. Magn. Reson*. 1986;67:258-266.
25. Melli TR, Scriven LE. Theory of two-phase cocurrent downflow in networks of passages. *Ind. Eng. Chem. Res*. 1991;30:951-969.

Manuscript received Oct. 9, 2003, and revision received June 2, 2004.